Emergent Materials (2025) 8:7327–7343
https://doi.org/10.1007/s42247-025-01172-y

ORIGINAL ARTICLE

Functionalization of nanostructured Niobium oxide with natural antioxidants for biomedical purposes

Pablo Araújo Oliveira[1] · Thaís Soares Farnesi-de-Assunção[1] · Isabela Sguilla Rotta[1] · Karina Ferrazzoli Devienne Vicentine[1] · Aline Dias Paiva[1] · Dayane dos Santos Alvares[2] · Marcio Daldin Teodoro[3] · Witor Wolf[4] · Jéferson Aparecido Moreto[4] · Natália Bueno Leite Slade[1]

Received: 13 December 2024 / Accepted: 22 June 2025 / Published online: 30 June 2025

Abstract

Niobium (Nb), a transition metal recognized for its chemical stability, corrosion resistance, and potential in biocompatible materials for biomedical use. Despite its advantages, its technological applications remain underexplored. In this context, the present study aims to broaden the applications of niobium by synthesizing and functionalizing nanostructured niobium oxide with distinct natural antioxidants, including ascorbic acid, tannic acid, and quercetin. This approach is based on the synergistic properties of these biomolecules, which exhibit antimicrobial, antifungal, and anticancer properties. When combined with the inherent properties of niobium, this strategy is expected to produce unprecedented and innovative nanostructured systems for biomedical purposes. Non-functionalized and functionalized samples were characterized regarding their electrical charge properties, morphology, structure, and crystallinity using techniques such as Zeta potential analysis, Scanning-Transmission Electron Microscopy, Scanning Electron Microscopy coupled with Energy Dispersive X-ray Spectroscopy, Fourier Transform Infrared Spectroscopy, Raman Spectroscopy, and X-ray Diffraction. The results indicate the successful formation of nanostructured materials based on hydrated niobium pentoxide, a characteristic that was preserved even after functionalization with the antioxidant compounds. Cell viability assays demonstrated that samples functionalized with antioxidants exhibit reduced interference with cell viability compared to their non-functionalized counterparts. Furthermore, the nanostructured systems were evaluated for their antibacterial properties, demonstrating both bactericidal and antibiofilm activities against *Escherichia coli* ATCC 25922. The synthesis and functionalization of nanostructured niobium materials, as proposed in this study, present a promising strategy for expanding the application of niobium in pharmaceutical and nutraceutical fields.

Keywords Nanostructured materials · Niobium · Functionalization · Natural antioxidants · Biomedical applications

1 Introduction

Niobium (Nb), a transition metal known for its excellent chemical stability, corrosion resistance, and biocompatibility, has emerged as a promising material for diverse applications, particularly in the biomedical field. Although its technological potential remains largely untapped, niobium's unique properties, including high thermal and electrical conductivity, malleability, and resistance to both localized and global corrosion, make it an attractive material for cutting-edge advancements across a range of innovative applications [1, 2]. Brazil, particularly the Triângulo Mineiro region of Minas Gerais, holds the largest global niobium reserves, with the Barreiro Mine, located in the city of Araxá, contributing approximately 80% of the world's total production

✉ Natália Bueno Leite Slade
natalia.slade@uftm.edu.br

1 Federal University of Triângulo Mineiro (UFTM), Uberaba, Minas Gerais, Brazil

2 São Paulo State University (UNESP), São José do Rio Preto, São Paulo, Brazil

3 Federal University of São Carlos (UFSCar), São Carlos, São Paulo, Brazil

4 University of São Paulo (USP), São Carlos, São Paulo, Brazil

[3]. Despite the established use of niobium in industrial sectors particularly in metallurgy (e.g., ferro-niobium alloy production), its potential integration into advanced biomedical technologies remains largely underexplored.

Recent studies have shown that niobium-based materials exhibit low cytotoxicity and promising antimicrobial properties, suggesting their potential in applications ranging from wound healing to dental materials [1, 2, 4–9]. In this context, nanostructured niobium oxide has stood out for its particular characteristics and potential applications in pharmaceutical products, biomaterials and other biomedical areas. However, a gap remains in the development of niobium-based nanoparticle systems, particularly those that integrate the metal's inherent properties with bioactive compounds. In this sense, the present study proposes innovative and applied research that aims to explore the bioactivity of pure and functionalized nanostructured niobium oxide, with distinct natural antioxidants: ascorbic acid (AA), tannic acid (TA), and quercetin (QUE).

These antioxidant compounds exhibit a wide range of biofunctional properties, including activity against neurodegenerative diseases, cancers, and bacterial infections [10–18]. They differ significantly in molecular size, electrostatic properties, and water solubility. Despite this, they share common challenges in achieving effective therapeutic and/or nutraceutical applications, primarily due to their low bioavailability. This limitation arises from their susceptibility to degradation in physiological environments, poor absorption, and ineffective targeting [19–23]. These limitations have persisted since their initial discovery [20, 23], but nanotechnology has emerged as a promising strategy for overcoming them. It offers the potential to protect the active compounds, enable controlled release, enhance absorption within the organism, and reduce production costs of formulations [23–33]. In this context, the strategy adopted in the present study advances the application of niobium-based technologies while facilitating effective incorporation of these biomolecules for healthcare applications.

For this, niobium oxide-based nanostructures were synthesized using the hydrolysis method [34–37]. This approach is widely employed for the production of metallic oxides due to its simplicity, cost-effectiveness, scalability, energy efficiency, and ability to produce high-purity and homogeneous final materials [38–41]. These advantages make the hydrolysis method a practical and efficient choice for the synthesizing niobium oxide nanoparticles, especially when a cost-effective and efficient process is required for technological and industrial applications. The resulting nanostructures were immersed in solutions containing the antioxidants and, then submitted to a comprehensive characterization, including Zeta potential analysis, Transmission Electron Microscopy (TEM), Scanning Electron Microscopy (SEM) coupled with Energy Dispersive X-ray Spectroscopy (EDX), Fourier Transform Infrared Spectroscopy (FTIR), Raman Spectroscopy, and X-ray Diffraction (XRD), to investigate the morphology, structure, and electrical properties of the synthesized materials. Additionally, the bioactivity of both functionalized and non-functionalized niobium oxide samples was evaluated through cell viability assays and antibacterial tests. The results demonstrated promising outcomes, including low toxicity, as well as significant bactericidal and antibiofilm activities against *Escherichia coli* ATCC 25922. The findings of this study highlight the potential of niobium-based nanostructured materials as multifunctional platforms for a broad spectrum of biomedical applications. These results pave the way for the development of novel therapeutic strategies that integrate the unique physicochemical properties of niobium with the bioactivity of natural antioxidants. This work not only broadens the scope of niobium utilization in advanced technological applications, but also has significant implications for both pharmacological and nutraceutical sectors.

2 Experimental

2.1 Materials

Niobium pentachloride, tannic acid, ascorbic acid, quercetin, and other reagents were purchased from high-grade analytical suppliers.

2.2 Synthesis of nanostructured Niobium oxide

Nanostructured niobium oxide (Nb-nano) was synthesized by dissolving the precursor ($NbCl_5$) in deionized water at 25 mg mL^{-1}. Upon dissolution, the yellow powder immediately turned white. The mixture was kept under magnetic stirring for 24 h at room temperature. Subsequently, the resulting white solid was separated by centrifugation at 4000 rpm for 15 min, washed thoroughly deionized water, and dried in an oven at 80 °C [36, 37]. At the end of the process, the material was ground and weighed.

2.3 Functionalization of Niobium nanostructures

The non-functionalized material was synthesized as described in Sect. 2.2. Subsequently, 15 mL of deionized water was added to the material. Then, AA and TA (diluted in 1 mL of deionized water) and QUE (diluted in 1 mL of absolute ethanol), at 2% of the Nb-nano mass, were added to the nanostructured niobium oxide solution during a 10-minute ultrasonic bath. The mixtures were magnetically stirred for 24 h at room temperature and protected from

light. The obtained solids were separated by centrifugation at 4000 rpm for 15 min, washed thoroughly deionized water, and dried at 80 °C [42, 43]. At the end of each process, the materials were ground and weighed, obtaining three nanostructured systems: Nb-AA, Nb-TA, and Nb-QUE.

2.4 Optical and structural characterizations of functionalized and non-functionalized Niobium nanostructures

Ultraviolet-visible spectroscopy (UV-Vis) was employed to evaluate the spectroscopic properties of the synthesized nanostructured systems, both functionalized and non-functionalized. UV-Vis scans were conducted using a UV-Vis spectrophotometer (Shimadzu UV 1800, Shimadzu Corporation, Kyoto, Japan) in the wavelength range of 190 to 500 nm. The samples were prepared at a concentration of 2 mg mL^{-1} and subjected to ultrasonic bath treatment for 1 h to enhance the dispersivity of the systems. All spectra were recorded at final concentration of 0.26 mg mL^{-1}. Infrared Spectroscopy with Fourier Transform (FTIR) measurements were performed on a spectrophotometer ALPHA II (Bruker Corporation, Massachusetts, USA) ranging from 4000 to 400 cm^{-1}, with a resolution of 4 cm^{-1} [37]. Raman scattering measurements were performed at room temperature using a homemade confocal microscope, with the samples being excited with a 532 nm diode laser (Cobolt / 08) focused on a spot of 1 µm with a power of 2 mW. The signal was dispersed by a 75 cm spectrometer and detected by a Silicon CCD (Andor Shamrock/Idus). X-ray diffraction (XRD) technique was used to investigate the crystallinity of the obtained materials. XRD analyses were performed on XRD-6100 diffractometer (Shimadzu Corporation, Kyoto, Japan) with a Cu Kα radiation source, operating at 40 kV and 30 mA, at angles between $5° < 2\theta < 80°$, with a rate of 1°/min and a step size of 0.01° [34].

2.5 Morphological characterizations of functionalized and non-functionalized Niobium nanostructures

The morphology and chemical composition of each sample were analyzed using Scanning Electron Microscopy. For this purpose, a JEOL-JSM7001F electron microscope, equipped with an energy-dispersive X-ray spectrometer (EDX) in SE (secondary electrons) and BSE (backscattered electrons) modes was used, operating at a voltage of 20 kV [44]. For the analysis, all samples were metalized with gold nanoparticles to ensure better electronic conduction of the studied systems and consequently higher resolution micrographs. The morphology of the nanostructures was also analyzed by Scanning-Transmission Electron Microscopy (STEM), using a FEI Magellan 400 L, Scanning Electron Microscope (SEM) with a Field Emission Gun (FEG) source, operating at 30 kV, equipped with a STEM detector. Prior to STEM observation, the samples were diluted in ethyl alcohol and then subjected to an ultrasonic bath to disperse the nanostructures which were subsequently deposited in a carbon-coated Cu-grit. Micrographs were taken with the Bright-Field (BF) and Dark-Field (DF) modes using the STEM detector and also using a Secondary Electron (SE) detector.

2.6 Charge properties of functionalized and non-functionalized Niobium nanostructures

Zeta potential measurements were performed using a Zeta-Sizer Nano ZS90 equipment (Malvern Instruments Ltd, UK) to verify the stability and surface charge of the synthesized systems. For analysis, the samples were diluted in deionized water (1% Tween 80) and treated in an ultrasonic bath. The measurements were performed using DTS 1060 cuvettes (Malvern) equipped with gold electrodes, employing Doppler velocimetry experiments to determine the zeta potential [32, 45].

2.7 Evaluation of the toxicity of functionalized and non-functionalized nanostructures

2.7.1 Cytotoxicity tests

Following synthesis, both the functionalized and non-functionalized materials, as well as the isolated antioxidants, were exposed to UV irradiation (254 nm) for 30 min followed by immersion in a water bath at 63ºC for 60 min to ensure sterility. Subsequently, they were resuspended in DMSO at a final concentration of 5 mg mL^{-1} and subjected to ultrasonic bath for 15 min to ensure complete dissolution of the nanomaterial. Biological assays were then performed.

The evaluation of cell biocompatibility was conducted in accordance with the guidelines outlined in the regulatory standard ISO 10993-5:2009 [46]. VERO-CCL81 cells were plated in 96-well plates (10^4 cells/well) and incubated for 24 h in an atmosphere at 37 °C and 5% CO_2. Then, the cells were placed in contact for 24 h with different concentrations of niobium-based nanoformulations (0–500 µg ml^{-1}), and subjected to the neutral red uptake test. The concentration of isolated antioxidants corresponds to 2% of the concentration of the associated nanostructures. This assay promotes the staining of lysosomes in viable cells and consequently provides a quantitative estimate of the number of viable cells. The cell viability was assessed by measuring absorbance at 540 nm using a microplate reader (ThermoPlate TpReader, USA). The percentage of viability was calculated relative to

untreated control cells. All tests were performed in triplicate and in independent experiments to ensure reproducibility.

2.7.2 Interference of nanostructured systems on bacterial growth and biofilm formation

The influence of both the antioxidants and the nanostructured systems on bacterial growth was evaluated using the broth microdilution technique. Different concentrations (2,500 to 156.25 μg mL^{-1}) of niobium-based nanostructures or pure antioxidants (equivalent to 2% of its corresponding nanostructure concentration (50 to 3.125 μg mL^{-1}) were added (50 μL) to 96-well plates containing BHI broth (2x concentration; 50 μL). Suspensions of stationary-phase *Escherichia coli* culture (10^6 CFU/mL; 10 μL) were added to the plates, and incubated at 37 °C for 24 h under aerobic conditions. Uninoculated BHI broth was used as negative control and medium inoculated only with the bacterium as positive growth control. The minimum inhibitory concentration (MIC) was defined as the lowest concentration at which bacterial growth was completely inhibited [47].

The minimal bactericidal concentration (MBC) of the antioxidants and the niobium-based nanostructures was determined following the MIC tests by transferring aliquots (5 μL) from wells with concentrations equal to or greater than the MIC onto plates containing BHI medium, in the absence of nanostructured systems/bioactive compounds. The plates were incubated at 37 °C for 24 h under aerobic conditions. The MBC was defined as the lowest concentration that prevented growth after subculturing in the absence of the test agent [48].

The ability of *Escherichia coli* to form biofilms in the absence and presence of the niobium-based nanostructures or the antioxidants was evaluated in polystyrene microplates using the crystal violet method. Briefly, stationary phase bacterial suspensions (0.5 McFarland; 10 μL) were added to 96-well plates already containing BHI broth (2x; 50 μL). Subsequently, each material was added at final concentration ranging from 2,500 to 156.25 μg mL^{-1}, with the concentrations of the isolated bioactive compounds corresponding to 2% of the respective nanostructured concentrations (50 μL), and the microplates were incubated at 37 °C for 24 h, under aerobic conditions. After this period, the microplates were treated with methanol (75%; 15 min), and after methanol evaporation, crystal violet solution (2%; 150 μL) was added. The microplates were maintained at room temperature for 15 min; the formed crystals were solubilized with ethanol (95%; 150 μL). The absorbance was measured at 540 nm in a microplate reader [49].

2.7.3 Statistical analysis

Statistical analysis was performed using Excel for Windows (Microsoft, USA) and GraphPad Prism® software version 8.0 (GraphPad, Inc., La Jolla, CA, USA). The results were analyzed based on the standard data distribution, demonstrating a Gaussian distribution. Therefore, the results were analyzed using ANOVA with Dunn's post hoc and expressed as mean and standard deviation. Differences were considered statistically significant when $p < 0.05$.

3 Results and discussion

3.1 Optical and spectroscopic characterization

The optical properties of the synthesized niobium-based materials were investigated using UV-Vis spectroscopy. To enhance solubility and dispersion, the samples were subjected to ultrasonication in a solution of deionized water and Tween 80 (1%), addressing their low intrinsic solubility. This approach aligns with previous methods by Odzak et al. [50] and Studer et al. [51] for dispersing and dissolving metal oxides in deionized water or water/Tween mixtures. Figure 1 illustrates the UV-Vis spectral behavior of the synthesized niobium-based materials, revealing a shoulder around 265 nm and a prominent peak near 310 nm, which are consistent with the spectral features of niobium pentoxide (Nb_2O_5) as reported by Chen et al. [52]. This spectral profile is attributed to both the crystalline Nb_2O_5 phase and the amorphous hydrated niobium oxide phase, $Nb_2O_5 \cdot nH_2O$, as described by Fuchigami and Kakimoto [53]. For the functionalized structures also shown in Fig. 1, the spectral pattern of the non-functionalized niobium sample remains largely preserved, maintaining the core characteristics of niobium pentoxide. However, samples Nb-AA and Nb-TA display a slight blue-shift in maximum absorbance, while Nb-QUE exhibits distinct peaks characteristic of QUE. Specifically, Nb-QUE shows two absorption maxima: the first, between 300 and 400 nm, corresponds to the cinnamoyl system associated with the conjugation of ring B and the carbonyl of ring C; the second, between 240 and 300 nm, corresponds to the benzoyl system associated with conjugation between ring A and the carbonyl of ring C [54]. The variations in maximum absorbance observed across samples are likely due to the differences in the bioactive agents used, as well as resulting variations in nanostructure size and morphology [55]. Smaller particle sizes, as observed in the functionalized samples, can contribute to the observed blue-shift effect [52]. Differences among the functionalized systems may also arise from the solubility properties of the antioxidants; for example, QUE, due to its

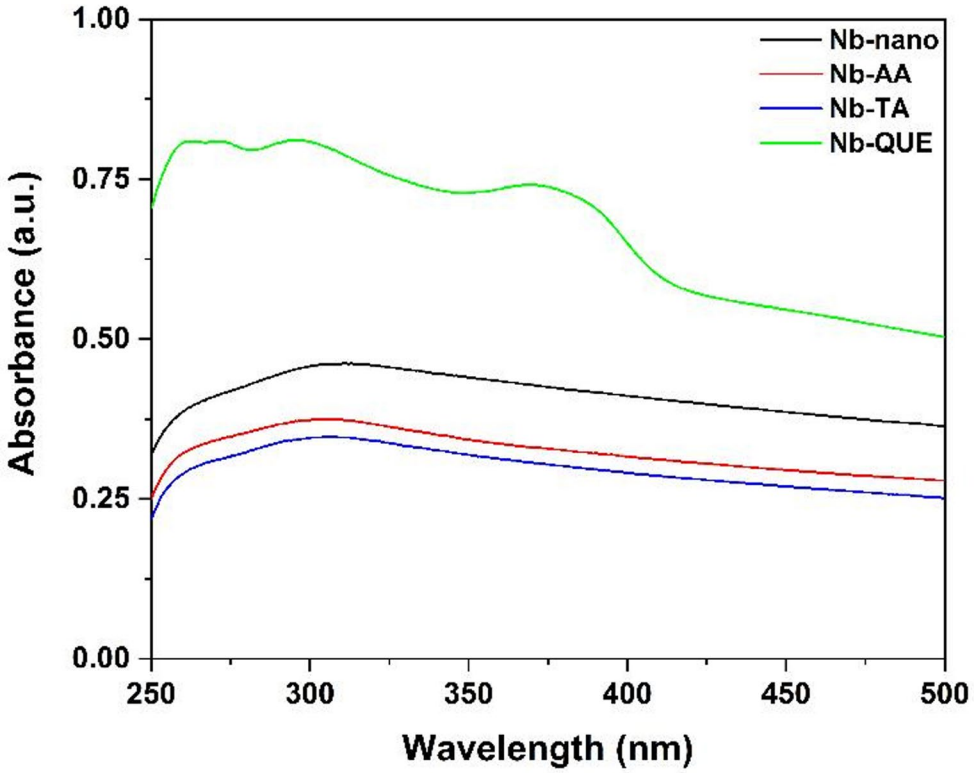

Fig. 1 UV-Vis spectra of the non-functionalized sample (Nb-nano) and the samples functionalized with AA (Nb-AA), TA (Nb-TA), and QUE (Nb-QUE)

low water solubility, may exhibit a stronger surface association with niobium oxide compared to more hydrophilic compounds. Additionally, the absence of specific bands for TA and AA could result from overlapping absorbance bands between niobium and these bioactives. The higher concentration of metallic material and the rinsing steps during synthesis may also have influenced these spectral variations. In summary, these findings confirm the effectiveness of the synthesis method in producing niobium-based materials and demonstrate that the functionalization process successfully preserved the core optical properties of niobium pentoxide.

The FTIR technique was used to obtain information about the structural parameters of functionalized and non-functionalized samples, as it allows the identification of specific and/or characteristic functional groups, as well as associated molecular interactions. Figure 2 displays the FTIR spectrum of the non-functionalized (Nb-nano) and the respective functionalized samples (Nb-AA, Nb-TA, and Nb-QUE). For Nb-nano (black lines), the band at 3048 cm^{-1} (Region A) may correspond to stretching vibrations of O-H bonds in water molecules incorporated in the sample [56], while the band at 1608 cm^{-1} (Region B) is probably associated with their bending vibrations [57, 58]. The band at 904 cm^{-1} (Region C) can be attributed to the vibrations of Nb=O bonds [37, 59, 60], whereas the band at 542 cm^{-1} (Region D) corresponds to Nb-O vibrations [37, 57]. The shoulder around 500 cm^{-1} observed in the FTIR spectra is consistent with findings reported by Skrodczky et al. [37]. While these authors do not associate it to any specific vibrational mode, Ferraro et al. shows that this region may be related to interactions between transition metallic oxides and water molecules [61]. The bands at 1230 and 1154 cm^{-1} can be attributed to residual organic components present in the material synthesis [57, 62]. Given that these results are consistent with those reported in FTIR spectra of hydrated niobium pentoxide-based materials [37, 56, 63], the characteristics of the Nb=O, Nb-O, and O-H bonds provide strong evidence supporting the identification of the material synthesized in this study as hydrated niobium oxide (or niobic acid), $Nb_2O_5{\cdot}nH_2O$. The FTIR spectra of the functionalized samples are also presented in Fig. 2(A–C), along with the spectra of the respective antioxidants in their isolated forms: AA (Fig. 2A), TA (Fig. 2B), and QUE (Fig. 2C). In general, Nb-AA, Nb-TA, and Nb-QUE exhibit similar patterns to the non-functionalized material. However, slight differences can be observed in the spectra of each functionalization. Notably, there is evidence of the persistence and even intensification (for Nb-AA) of the bands associated with C–O bond vibrations, along with the emergence of new bands corresponding to the bending vibrations of C–H bonds and C=C vibrations of aromatics groups, particularly in the case of Nb-QUE [62, 64]. The bands observed in the regions between 1600 and 1400 cm^{-1} and 1300–1000 cm^{-1} are indicative of the successful incorporation of bioactive compounds into the nanostructures, thereby confirming the functionalization of the materials with the antioxidant agents

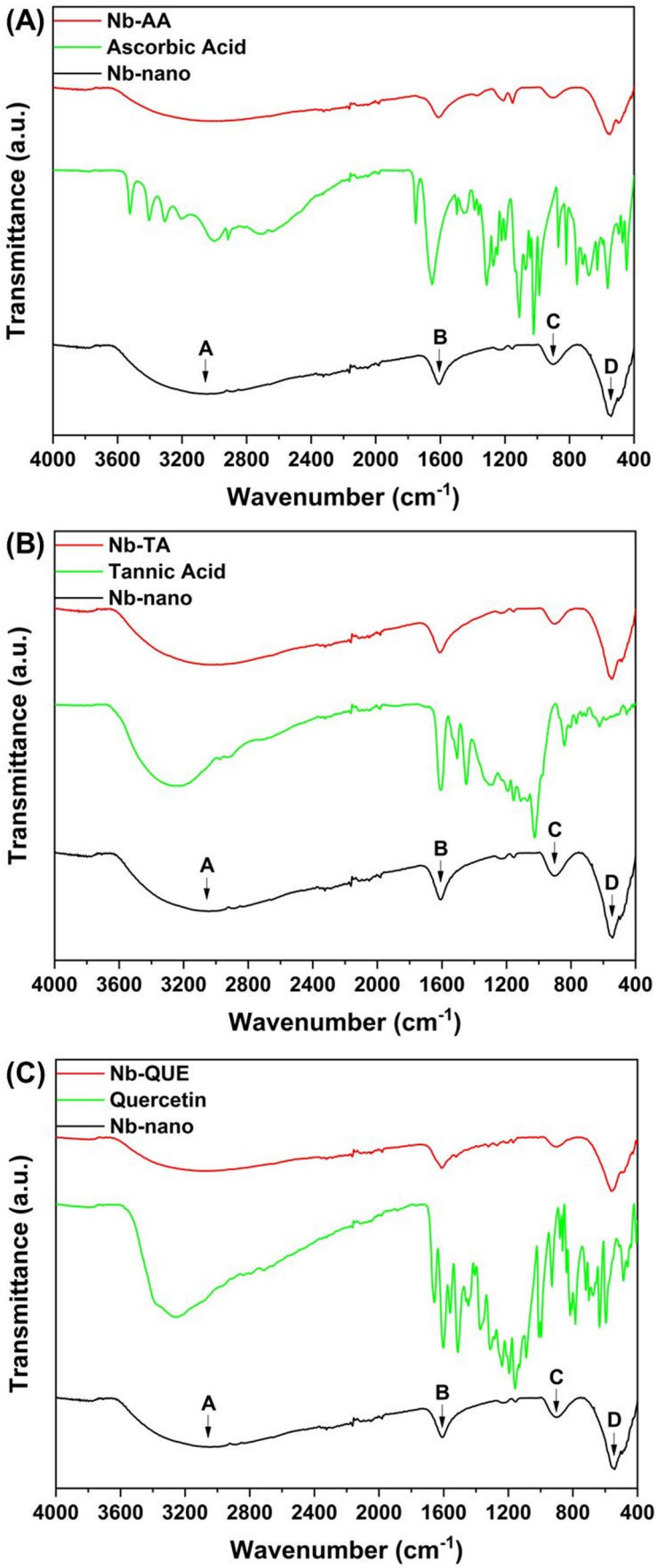

Fig. 2 FTIR spectra of the non-functionalized sample (Nb-nano) and the samples functionalized with (**A**) AA (Nb-AA), (**B**) TA (Nb-TA), and (**C**) QUE (Nb-QUE), along with the spectra of their respective antioxidants in isolated form

ascorbic acid (AA), tannic acid (TA), and quercetin (QUE). A similar observation was reported by Shah et al. [42] during the functionalization of iron oxide nanoparticles with gallic acid, as well as during the subsequent use of quercetin (QUE) for magnetite functionalization [43]. While the literature is well-established with regard to the synthesis of niobium-based nanostructured materials for electrical and optical applications, their exploration for biomedical purposes has only recently begun to garner increasing scientific interest. For instance, Brum et al. [65] reported the green synthesis of niobium nanoparticles using pecan nutshell extract (*Carya illinoinensis*) to evaluate its antioxidant activity. In their study, the ATR-FTIR spectrum of the resulting Nb_2O_5 nanoparticles displayed a band near 1000 cm^{-1}, attributed to the C–O stretching vibrations of phenolic and polyphenolic compounds present in the extract, an observation that is in agreement with the findings reported here. Green synthesis typically employs natural biological extracts or supernatants as reducing agents in place of conventional chemical reagents. These biological sources are rich in enzymes, amino acids, proteins, and flavonoids, which contribute to the reduction of metal ions and promote nanoparticle formation. In contrast, the present study utilizes bioactive compounds after the synthesis step, with the aim of promoting the surface functionalization of the nanostructures with well-known antioxidant agents. This strategy is intended to enhance the biological potential of the resulting materials. This methodological difference explains the greater number of infrared absorption bands associated with organic compounds observed in our samples, as compared to the results reported by Brum et al. [65], and underscores the novelty of the approach adopted in this work. To the best of our knowledge, this is the first study to report the synthesis of niobium-based nanostructures functionalized with bioactive compounds. Furthermore, the results indicate that the functionalization process does not alter the fundamental structural characteristics of the synthesized material, as also corroborated by the UV–Vis spectroscopy data.

Raman spectroscopy was employed to further complement the structural characterization of the synthesized materials, with the results presented in Fig. 3. All samples exhibit broad bands, indicative of an amorphous or poorly crystalline structure [66]. Both functionalized and non-functionalized materials display a band near 215 cm^{-1}, attributed to the bending mode of Nb–O–Nb bonds [37, 66], while the band at approximately 650 cm^{-1} corresponds to the stretching mode of Nb–O–Nb bonds [66]. Additionally, the bands between 800 and 1000 cm^{-1} are associated with Nb=O bonds in distorted structures, likely resulting from the coordination of water molecules [37]. These spectral characteristics were similarly observed in hydrated niobium pentoxide-based materials, as demonstrated by Skrodczky et al. [37], Bousada et al. [63], Jehng and Wachs [67], and Lebarbier, Houalla and Onfroy [68]. Functionalization induced variations in the Raman spectra, with the emergence of new bands. For Nb-AA, a new band around 1624 cm^{-1} is attributed to the stretching mode of C=C bonds in ascorbic acid (AA) [69, 70]. Similarly, for Nb-TA, a new band near 1608 cm^{-1} is associated with the stretching mode of C=O bonds in the benzene ring of tannic acid (TA) [71]. In the case of Nb-QUE, the Raman spectrum reveals a new band around 1583 cm^{-1}, corresponding to the stretching mode of the C=O bond in the carbonyl group, alongside two additional bands at approximately 1488 and 1344 cm^{-1}, which are linked to the bending mode of O–H bonds in quercetin (QUE) [43, 72]. These spectral variations align with the results obtained from FTIR analysis, indicating that the functionalization process did not significantly alter the fundamental structure of the materials. Additionally, it also indicates the presence of bioactive compounds, demonstrating the successful functionalization of the materials.

The crystallinity of the obtained materials was investigated using X-ray diffraction (XRD). The results are displayed in Fig. 4, which presents the XRD patterns of the non-functionalized and functionalized samples. It is possible to observe the presence of two broad diffraction peaks at approximately 25° and 54°, which are consistent with those reported by Marin et al. [36], Fan et al. [34], and Rodrigues [60] for hydrated niobium pentoxide ($Nb_2O_5 \cdot nH_2O$). The absence of well-defined diffraction peaks is characteristic of amorphous materials [36, 37, 52, 57, 60, 65], and it also can be attributed to particles with extremely small sizes, as reported by Skrodczky et al. [37]. Similar XRD patterns were obtained for the Nb-nano samples functionalized with AA, TA, and QUE. Nb-AA exhibits a slight peak around 18°. For Nb-TA and Nb-QUE, no significant changes are observed in their XRD patterns when compared to the non-functionalized material. Consistent with the findings of Shah et al. [42, 43], our results demonstrate that the functionalization did not alter the phase of niobium oxide. All synthesized materials exhibited low crystallinity, indicating an amorphous structure.

3.2 Morphological characterization

A morphological characterization of the synthesized materials was conducted using scanning (SEM) and transmission electron microscopies (TEM). Figure 5A displays the SEM micrograph obtained for the non-functionalized Nb-nano. The figure clearly shows that the obtained material is composed of agglomerates of particles with nanometric dimension, similar to those reported by Rodrigues [60] for $Nb_2O_5 \cdot nH_2O$ synthesized from metallic niobium.

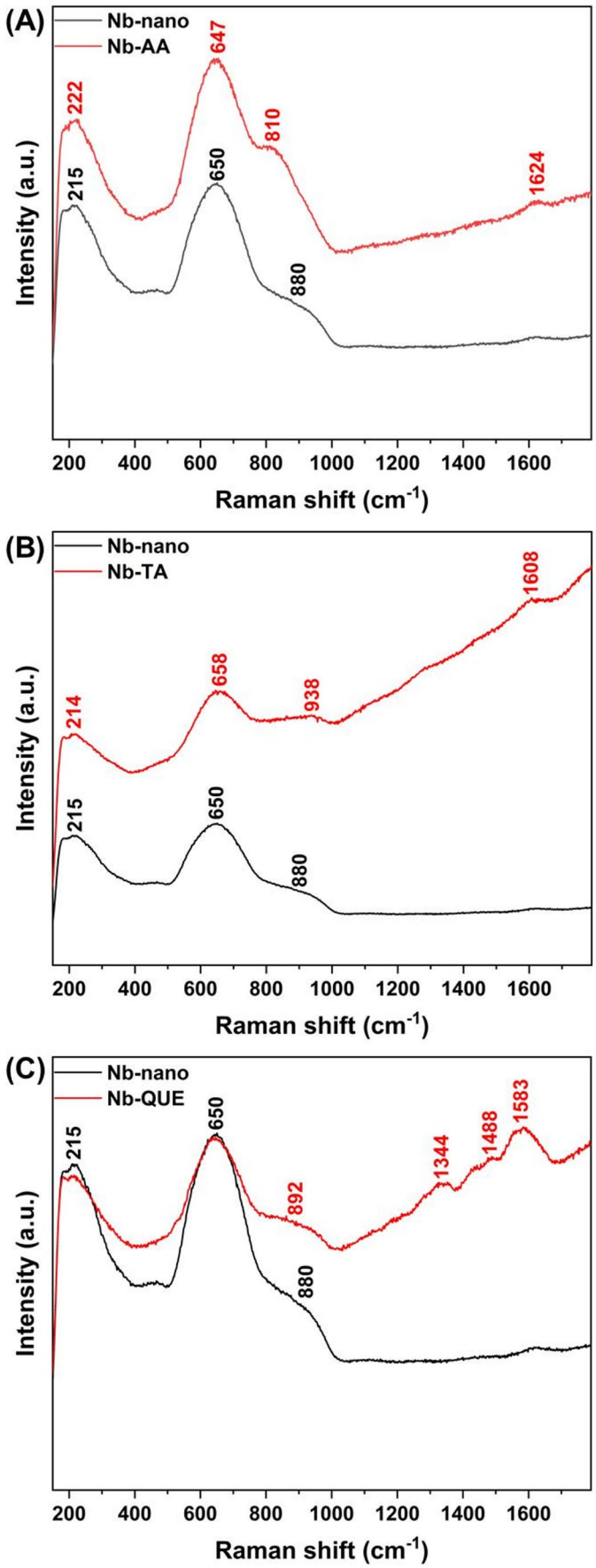

Fig. 3 Raman spectra of the non-functionalized sample (Nb-nano) and the samples functionalized with (**A**) AA (Nb-AA), (**B**) TA (Nb-TA), and (**C**) QUE (Nb-QUE)

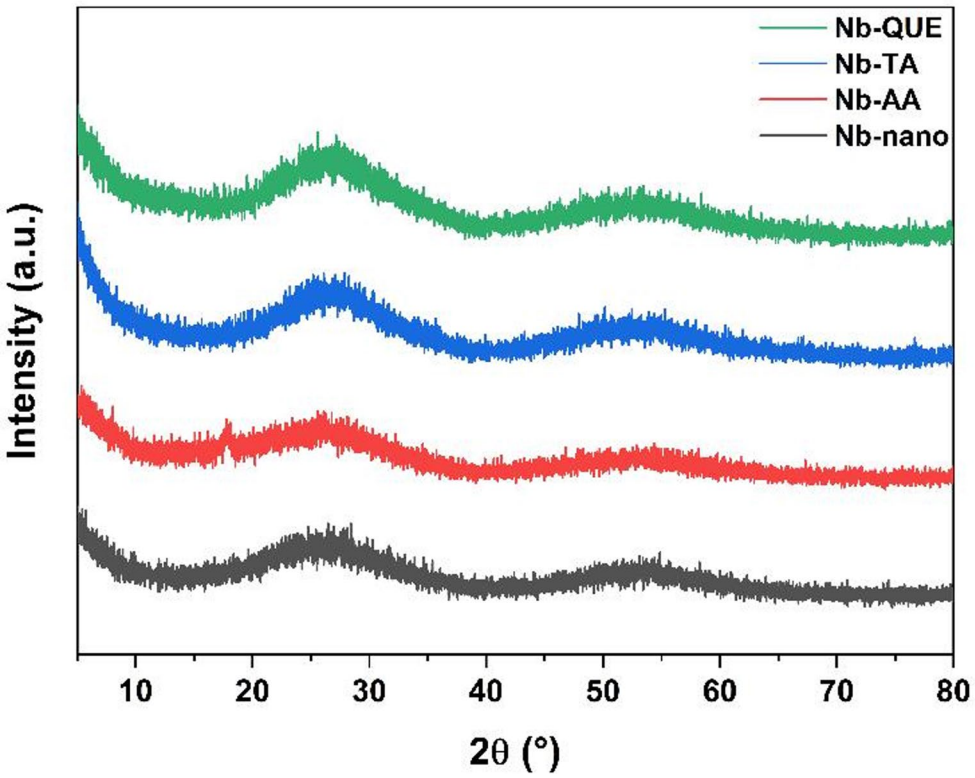

Fig. 4 X-ray diffraction (XRD) patterns of the non-functionalized sample (Nb-nano) and the samples functionalized with AA (Nb-AA), TA (Nb-TA), and QUE (Nb-QUE)

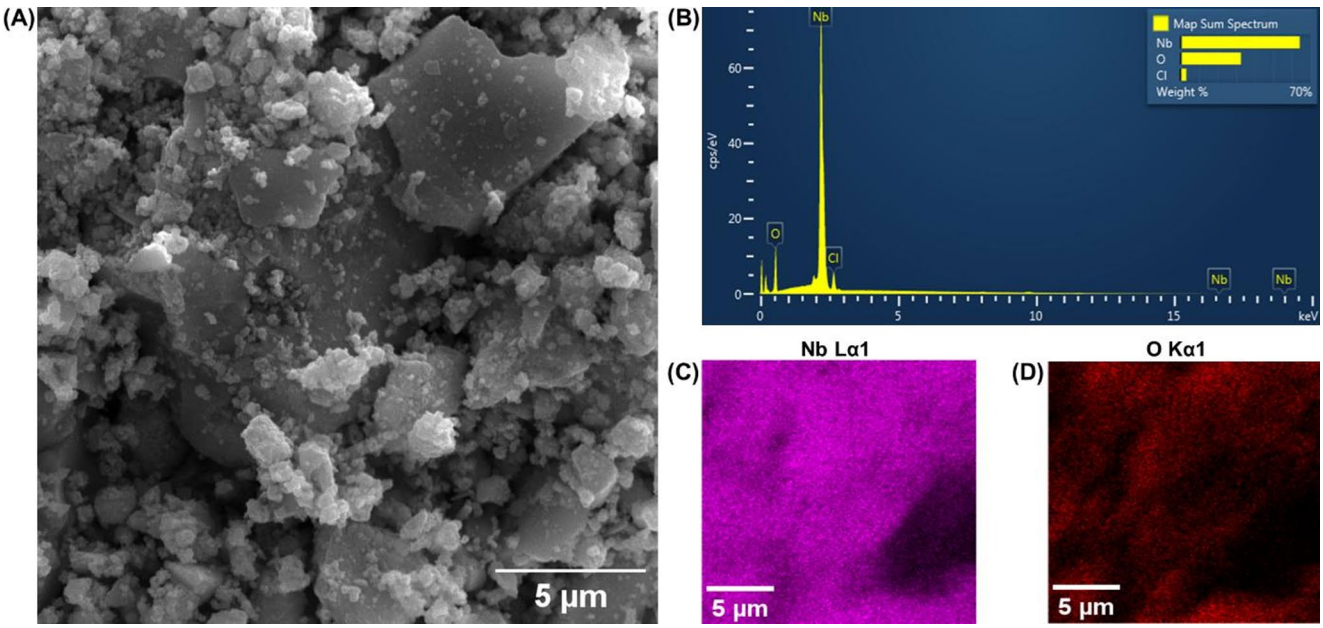

Fig. 5 (**A**) SEM image of the Nb-nano sample. (**B**) EDX spectrum of the analyzed sample, in which (**C**) is niobium and (**D**) is oxygen. Magnification: 10,000x

In the referenced study, samples were synthesized using the reverse microemulsion method, and TEM analysis revealed the presence of agglomerates smaller than 50 nm. However, individual particle sizes could not be distinctly identified. Figure 5(B-D) presents the chemical composition analysis obtained through Energy Dispersive X-ray Spectroscopy (EDX), based on the micrograph exhibited in Fig. 5A. This result reveals the chemical elements present in the sample, along with an estimation of their concentration in atomic weight%. This data contributes to confirming the synthesis of a material based on an oxide of niobium. The presence of chlorine (Cl) must

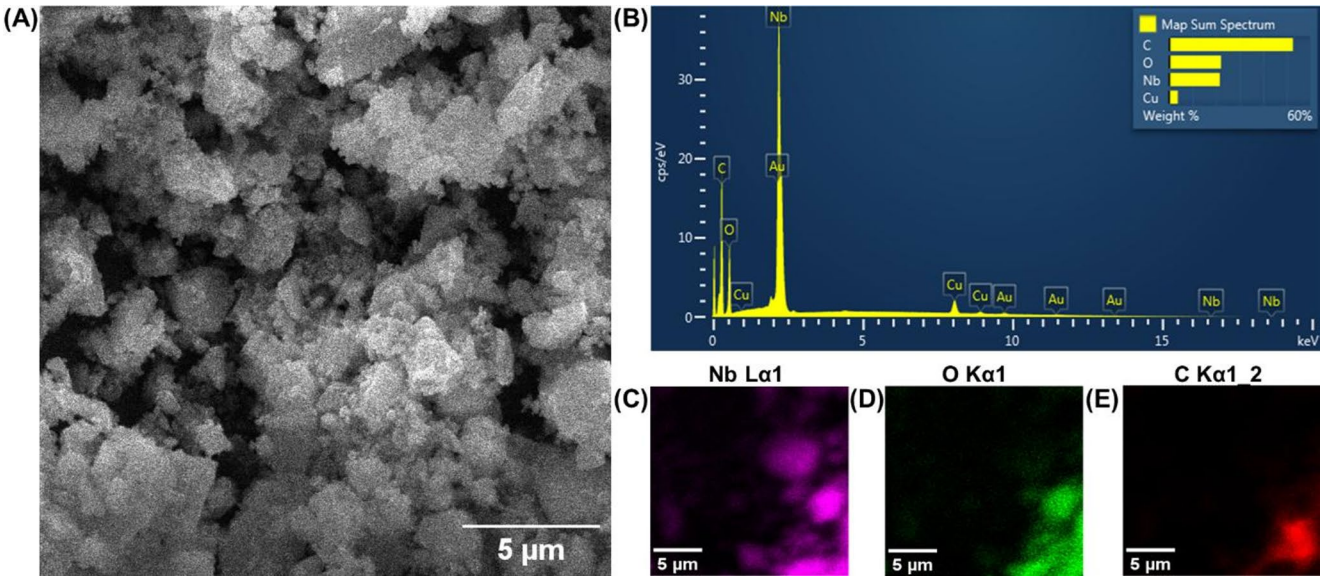

Fig. 6 (**A**) SEM image of the Nb-nano sample functionalized with QUE, Nb-QUE. (**B**) EDX spectrum of the analyzed sample, in which (**C**) is niobium, (**D**) is oxygen, and (**E**) is carbon. Magnification: 10,000x

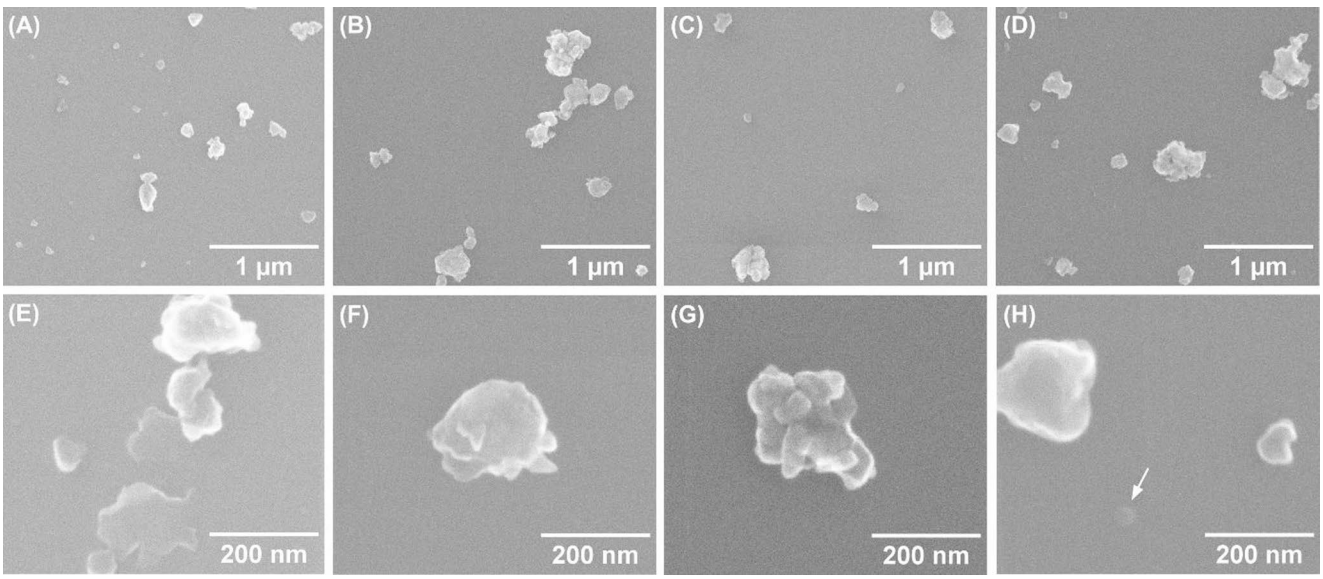

Fig. 7 STEM images in SE mode of the Nb-nano samples: (A) non-functionalized and functionalized with (B) AA, (C) TA, and (D) QUE, magnification of 100,000x; and (E) non-functionalized and functionalized with (F) AA, (G) TA, and (H) QUE, magnification of 500,000x

be attributed to trace amounts of the precursor material ($NbCl_5$) which remained in the sample despite the washing process.

The SEM micrograph of the Nb-nano functionalized with QUE is shown in Fig. 6A, exhibiting a morphological appearance similar to that of the non-functionalized Nb-nano. Nanometric-scale agglomerates are again observed, although the exact shape of the synthesized material cannot be distinctly defined. However, it can be noted that the functionalization process did not affect the morphological characteristics of the material. Figure 6B-E display the chemical composition obtained via EDX for the analyzed region of the sample. In addition to niobium and oxygen, significant amounts of carbon and trace amounts of copper are present. The copper signal is likely due to the tape used in the sample holder during SEM analysis. The carbon signal is attributed to the QUE molecules [43], reinforcing the success of the functionalization process. The absence of chlorine may be linked to the additional washing steps applied to the functionalized samples compared to the non-functionalized ones. This behavior was consistently observed across all antioxidants studied.

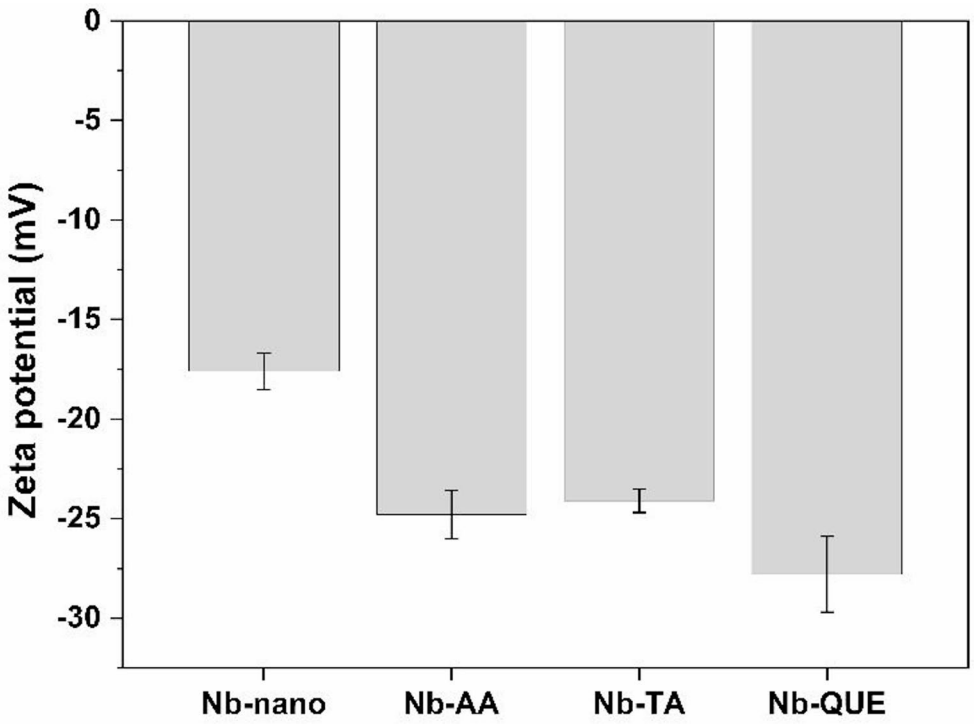

Fig. 8 Zeta Potential (ζ) measurements of the non-functionalized sample (Nb-nano) and the samples functionalized with AA (Nb-AA), TA (Nb-TA), and QUE (Nb-QUE)

STEM analysis was conducted on both functionalized and non-functionalized samples, with the corresponding images shown in Fig. 7. This analysis also reveals the presence of clusters of nanosized particles at the nanoscale, regardless of the functionalization process, where individual particles are not distinctly identified. This result is consistent with findings in the literature for hydrated niobium pentoxide obtained by the same methodology [34, 36, 37]. Furthermore, it was not possible to observe significant variations between functionalized and non-functionalized materials, nor even to establish a standard for the size of the clusters. However, the sample of the material functionalized with QUE (Fig. 7H) allowed for particle size estimation using ImageJ software, revealing diameters on the order of 30 nm (white arrow). This is slightly smaller than the crystalline niobium pentoxide nanoparticles obtained by thermal decomposition [73].

3.3 Charge properties

Figure 8 presents the zeta potential values for both non-functionalized and functionalized samples when dispersed in water. These data offer valuable insights into the surface charge characteristics of the synthesized materials, as well as their stability in aqueous dispersions. A higher zeta potential indicates stronger electrostatic repulsion between the nanostructures, which promotes better dispersion and minimizes aggregation in aqueous environments [32, 74]. Our results demonstrate that the non-functionalized sample (Nb-nano) exhibited an anionic nature with an average zeta potential of -17.6 mV. This value contrasts with those reported by Kumari and colleagues, who observed zeta potentials lower than −10 mV [74] and below −5 mV [75] for synthesized crystalline Nb_2O_5. In our study, the materials displayed more negative zeta potential values, especially for the functionalized Nb-nano samples. Functionalization appears to enhance electrostatic repulsion, thereby reducing agglomeration and improving system stability. This is supported by the zeta potential values observed: -24.8 mV for Nb-AA, -24.1 mV for Nb-TA, and −27.8 mV for Nb-QUE. This trend is consistent with the anionic nature of natural antioxidants at neutral pH [33]. These results may be attributed to the presence of bioactive compounds on the surface of the functionalized nanostructures, in line with the metal–antioxidant complex formation proposed by Barreto et al. [76], wherein hydroxyl groups on the surface of hydrated nanostructured niobium facilitate the attachment of functional moieties [43]. Therefore, the greater adsorption on the material's surface, the more negative the zeta potential value becomes [32]. However, it is important to note that the variation in zeta potential is not directly proportional to the net electric charge of the bioactive compounds, which at pH 7.4 are Q_{AA} = -1, Q_{TA} = -1.5, and Q_{QUE} = -0.7 [33]. This suggests that other factors may contribute to this variation, such as the amount of groups available for hydrogen bond formation and the differing solubilities of the bioactives, with AA and TA being hydrophilic compounds, while QUE is hydrophobic. The low solubility of quercetin was also

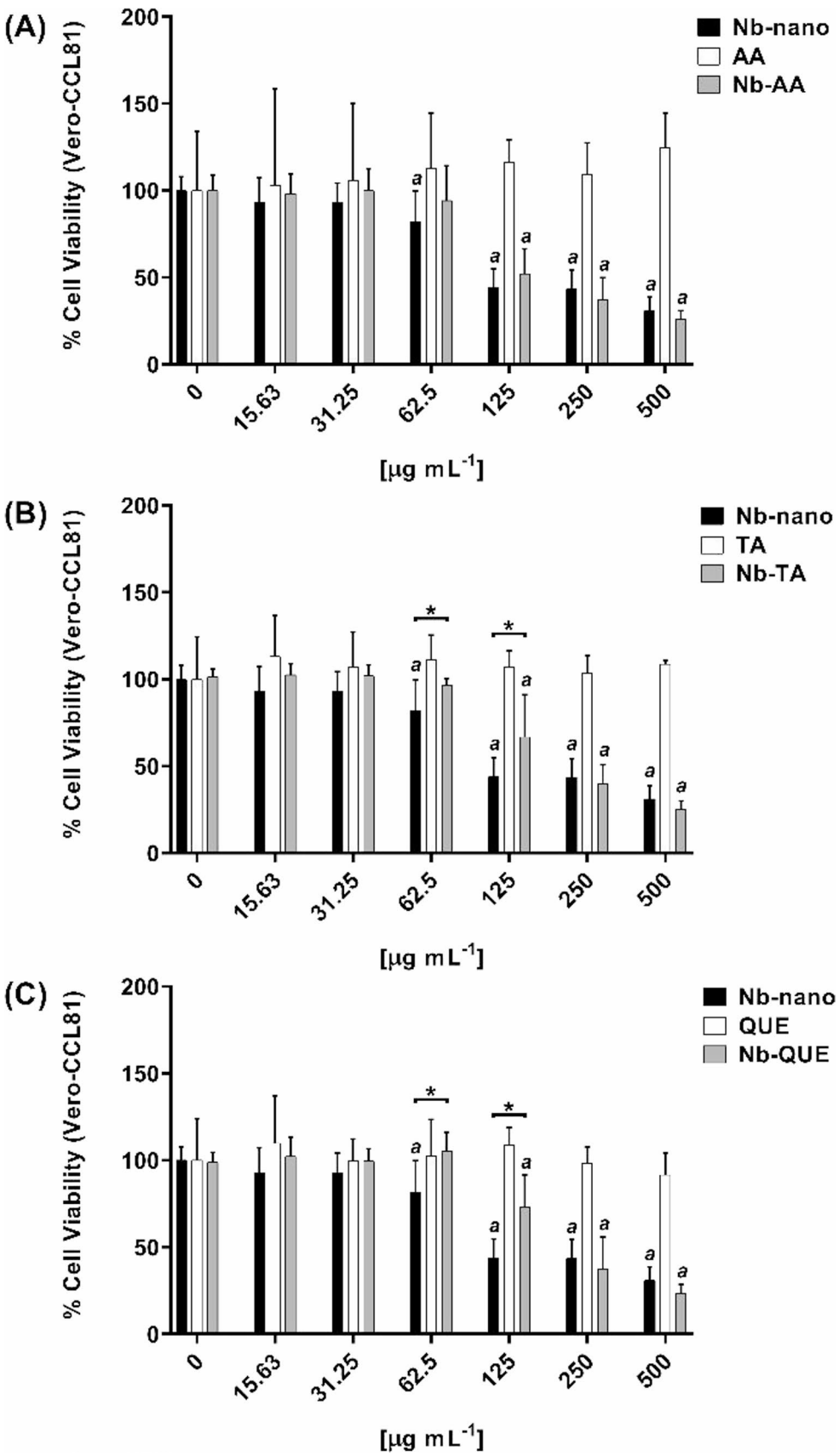

Fig. 9 Cell viability assay in Vero CCL-81 cells in the presence of Nb-nano and its functionalized forms: (**A**) AA, (**B**) TA, and (**C**) QUE, each accompanied by its respective isolated bioactive compound. The concentration of isolated antioxidants corresponds to 2% of the concentration of the associated nanostructures. Symbols: *a* $p<0.05$ versus control group; * $p<0.05$ between Nb-nano and Nb-functionalized forms

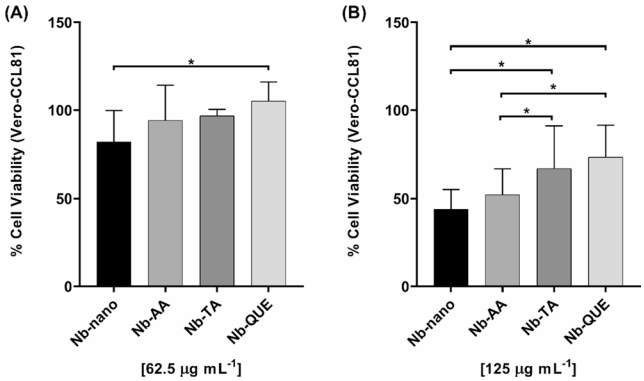

Fig. 10 Cell viability assay in Vero CCL-81 cells in the presence of Nb-nano, Nb-AA, Nb-TA, and Nb-QUE at concentrations of (**A**) 62.5 µg mL^{-1} and (**B**) 125 µg mL^{-1}. Symbol: * indicates a statistically significant difference ($p<0.05$) between the different nanostructures

used to justify the intensity of its absorption bands in the results obtained during the spectrophotometric characterization of the synthesized materials (**see** 3.1 section). Together, these results strongly suggest that the solubility characteristics of the bioactive compounds play a significant role in optimizing the functionalization process. Thus, the experimental approach employed in this study provides evidence that, among the functionalized materials, those containing quercetin (QUE) exhibit the highest antioxidant concentration compared to those functionalized with other bioactive compounds. This may be attributed to a favorable balance among molecular size, solubility, net charge, and hydrogen-bonding capacity, which collectively promote metal–ligand complex formation.

3.4 Cellular cytotoxicity of the synthesized nanostructures

In order to investigate the cytotoxicity of functionalized and non-functionalized niobium nanostructures, a biological study was carried out to evaluate the impact of different concentrations of these nanostructures on the viability of Vero CCL-81 cells in vitro. The results presented below express the percentage of cell viability in relation to the untreated control. Figure 9 presents the results of cell viability assay in Vero CCL-81 cells in the presence of Nb-nano, its functionalized forms and their respective isolated bioactive compounds: AA (Fig. 9A), TA (Fig. 9B), and QUE (Fig. 9C). The results show that the isolated antioxidants exhibit no cytotoxic effects at the tested concentrations, whereas the non-functionalized nanostructures (Nb-nano) display significant cytotoxicity at concentrations equal to or above 62.5 µg mL^{-1}. However, after functionalization with antioxidants, the Nb-AA, Nb-TA and Nb-QUE nanostructures demonstrate significant reduction in cell viability only at concentrations equal to or above 125 µg mL^{-1}. This effect

Table 1 Minimum inhibitory concentration (MIC) and minimum bactericidal concentration (MBC) of the nanostructured systems against *Escherichia coli* ATCC 25922

Nanostructured system	MIC (µg mL^{-1})	MBC (µg mL^{-1})
Nb-nano	1,250	2,500
Nb-AA	1,250	2,500
Nb-TA	625*	2,500
Nb-QUE	625*	2,500

*demonstrate statistical differences ($p<0.05$) regarding the non-functionalized material (Nb-nano)

may be attributed to the availability of bioactive sites on the surface of the nanostructures, which can interact with cell membranes. Given that the synthesized materials contain a significantly higher proportion of niobium relative to the antioxidant compounds, it is evident that, as the concentration increases, the cytotoxic effects associated with niobium begin to predominate in the overall biological response of the material.

Figure 10 exhibits the effects of nanostructures on the viability of Vero cells at the concentrations most relevant to this study, specifically those at which the activity of the functionalized nanostructures is enhanced compared to Nb-nano. At 62.5 µg mL^{-1} (Fig. 10A), a significant difference was observed only between Nb-nano and Nb-QUE. However, when these results are compared with the data obtained in the absence of nanostructures (Fig. 9) at the same concentration, it becomes evident that the reduction in cell viability occurred exclusively with the non-functionalized material. At the higher concentration of 125 µg mL^{-1} (Fig. 10B), both Nb-TA and Nb-QUE exhibited significant differences relative to Nb-nano by demonstrating higher cell viability in comparison to the non-functionalized material. In this sense, our results indicate that the cytotoxic effects associated with the functionalized materials (Nb-AA, Nb-TA, and Nb-QUE) were only evident above 125 µg mL^{-1}. These findings highlight the potential of functionalized nanostructures to improve biocompatibility by mitigating the cytotoxic effects related to non-functionalized niobium oxide. There are several mechanisms that may be involved in the reduction of cell viability; however, the first step for applications in biological systems is the evaluation of cytotoxic effects in vitro. The results presented here are consistent with other studies that explored the potential biological application of Nb_2O_5 in the modification and improvement of different materials, which demonstrated good biocompatibility and low cytotoxicity in their findings after niobium functionalization [1, 2, 4–9]. Dsouki and colleagues [77] conducted an in vivo study to investigate the cytotoxic, hematological and histological effects of niobium pentoxide in Swiss mice and their results suggest that Nb may be associated with acute inflammation but not with cell death. Inflammatory and pathological processes, such as cancer,

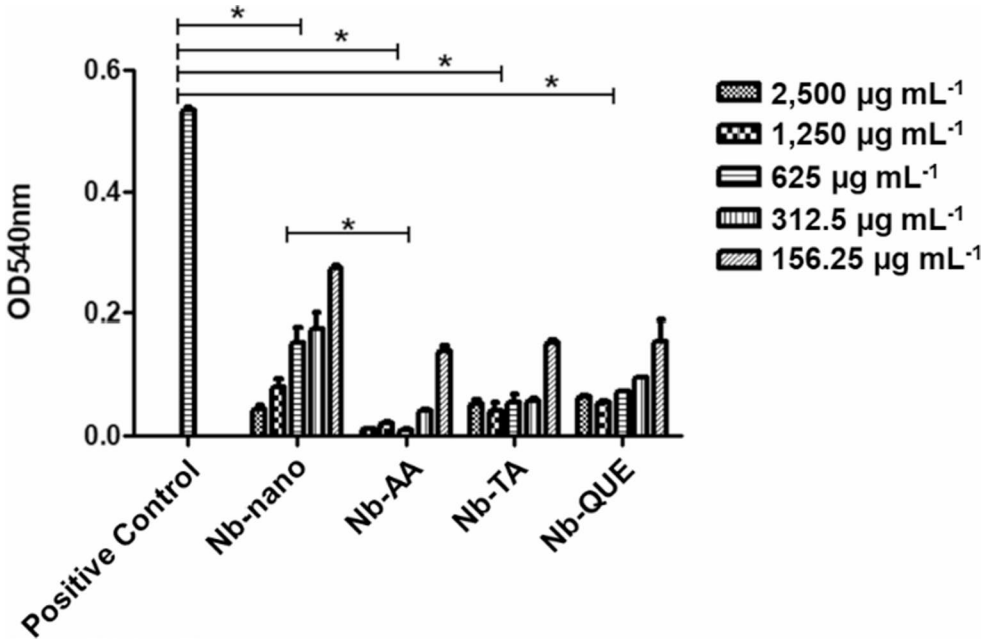

Fig. 11 Effect of non-functionalized (Nb-nano) and functionalized (Nb-AA, Nb-TA, Nb-QUE) systems on biofilm formation by *Escherichia coli* ATCC 25922. * demonstrate statistical differences ($p < 0.05$) regarding the positive control or the non-functionalized material (Nb-nano)

vascular diseases and arthritis, are associated with excess free radicals and reactive oxygen species that react with biologically active molecules and result in cellular damage and consequent homeostatic imbalance [78]. In contrast, antioxidant substances can neutralize, inhibit or delay the deleterious action of free radicals [79, 80]. Thus, our set of data on cellular cytotoxicity suggests that the biofunctionalization of niobium with antioxidant molecules interferes less with the viability of fibroblasts, making it a promising tool to be explored.

3.5 Interference of nanostructured systems on bacterial growth and biofilm formation

The MIC and MBC values for the nanostructured systems evaluated on *E. coli* ATCC 25922 are shown in Table 1. The assays with the isolated bioactive compounds were conducted with concentrations varying from 50 to 3.125 µg mL^{-1}, equivalent to 2% of its corresponding nanostructure concentration (2,500 to 156.25 µg mL^{-1}). At the concentrations evaluated, the antioxidant compounds did not exhibit inhibitory effects, and therefore, their MIC and MBC values could not be determined. Nanostructured niobium oxide showed MIC of 1,250 µg mL^{-1}. Nb-TA and Nb-QUE equally inhibited the growth of *E. coli* after 24 h of incubation, with recorded MICs of 625 µg mL^{-1}. Regarding Nb-AA, the MIC values recorded were twice (1,250 µg mL^{-1}) as high as those observed for the other functionalized nanostructures. The values observed for MBC for all the nanostructured systems (non-functionalized and functionalized) were 2,500 µg mL^{-1}. It can be concluded that functionalized material showed higher ability to antagonize bacterial growth when compared to the non-functionalized system, especially considering the antioxidants tannic acid and quercetin, as shown by the lower values for MIC ($p < 0.05$). These results are in line with those obtained for the niobium pentoxide thin films (Nb_2O_5) deposited on the surface of a Ti-6Al-4 V alloy, which showed antibacterial action against *Staphylococcus aureus* [4]. Similar effects have also been observed for other metal oxide nanoparticles functionalized with quercetin (QUE) and gallic acid [42, 43]. However, differences between the activity against Gram-positive and Gram-negative bacteria should be expected, considering the differences in their cell walls and the hypothesis that the activity of these nanostructures is associated with the destruction of membrane integrity [42, 43].

Biofilms are defined as structured microbial communities adhered to a solid surface and embedded in a polysaccharide matrix. Biofilms can be formed on natural or artificial surfaces, causing a series of problems, from the fouling of water processing equipment to persistent in vivo infections. An estimated 80% of chronic microbial infections in humans are thought to involve biofilm formation and persistence. Furthermore, biofilms are intrinsically linked with antimicrobial resistance to drugs, since the dense structure of the biofilm limits to antimicrobial agents, often resulting in treatment failure and recurrence of biofilm-related infections. Given this challenge, the development of novel strategies for biofilm prevention and management is critical. *E. coli* is a classic model for evaluating in vitro antibiofilm properties of a compound [81–83]. In order to assess the biological potential of the synthesized nanostructures, we evaluated the interference of the systems on biofilm formation by *E. coli*. Both functionalized and non-functionalized

niobium-based nanostructures effectively inhibited biofilm formation by *E. coli*, in a dose-dependent manner (Fig. 11). Even at the lowest concentrations evaluated (156.25 μg mL^{-1}), the antibiofilm activity of all nanostructured systems was maintained, and a reduction in biofilm formation ranging from 48.93 to 71.54% was observed when compared to the positive control (biofilm formed in the absence of nanostructured systems) ($p < 0.05$). In comparison to the non-functionalized material, Nb-AA showed a significant increase in the potential to inhibit biofilm formation by *E. coli* ($p < 0.05$) (Fig. 11). Regarding the isolated antioxidants, their activity was assessed at concentrations equivalent to 2% of those used in the corresponding nanostructures. At these concentrations (50 to 3.125 μg mL^{-1}), the compounds showed no inhibitory effect on biofilm formation.

Our findings support the hypothesis that the functionalization of niobium-based nanostructures with natural antioxidants imparts significant bioactive properties to the material, thereby broadening the potential applications of niobium in the biomedical field. The promising antibacterial activity observed highlights the novelty and effectiveness of these bioactive-surface materials, distinct from conventional encapsulated systems, and underscores their potential as advanced therapeutic platforms. Future investigations need to be focused on elucidating the underlying mechanisms of their biological activity, with the goal of fully harnessing the functional potential of these innovative nanostructured materials for future biomedical applications.

4 Conclusions

To the best of our knowledge, this is the first time that niobium nanostructures functionalized with bioactive compounds have been synthesized and subjected to biofunctional testing. The present study successfully demonstrated the synthesis and functionalization of nanostructured amorphous niobium pentoxide ($Nb_2O_5{\cdot}nH_2O$) pure and functionalized with natural antioxidants, including ascorbic acid, tannic acid, and quercetin. The functionalized and non-functionalized materials were characterized regarding their optical, spectroscopic, and morphological properties. The biofunctional properties of synthesized materials were also investigated. Cell viability assays demonstrated that antioxidant-functionalized samples exhibited significantly lower interference with cell viability compared to the non-functionalized ones. Antibacterial and antibiofilm activities against *Escherichia coli* highlight that the functionalization of the nanostructured niobium systems with the antioxidants in this study contributes to promoting their biological activity. These findings underscore the promising potential of niobium-based nanomaterials to be used in pharmaceutical and nutraceutical applications, offering a novel approach to leverage the synergistic properties of niobium and natural antioxidants for innovative biomedical solutions.

Author contributions Pablo Araujo Oliveira: Writing– original draft, Methodology, Investigation, Formal analysis. Thaís Soares Farnesi-de-Assunção: Cytotoxicity Tests, Formal analysis. Isabela Sguilla Rotta: Antibacterial and antibiofilm tests, Formal analysis. Karina Ferrazzoli Devienne Vicentine: Cytotoxicity Tests, Formal analysis. Aline Dias Paiva: Antimicrobial and antibiofilm tests, Formal analysis. Dayane dos Santos Alvares: Zeta Potential, Formal analysis. Marcio Daldin Teodoro: Raman spectroscopy, Formal analysis. Witor Wolf: Scanning-Transmission Electron Microscopy, Formal analysis. Jéferson Aparecido Moreto: Writing– review & editing, Funding acquisition, Formal analysis. Natália Bueno Leite Slade: Funding acquisition, Project administration, Writing– review & editing. All authors have read and agreed to the published version of the manuscript.

Funding Pablo A. Oliveira is grateful for the scholarship from the Foundation Coordination for the Improvement of Higher Education Personnel (CAPES - Finance Code 001). J. (A) Moreto would like to acknowledge the financial support received from the National Council for Scientific and Technological Development (CNPq-Brazil) (Grants 303659/2019-0, 402988/2021-3). N. (B) Leite is grateful for the financial support received from the CNPq-Brazil (Grant 405457/2023-5) and the Minas Gerais State Agency for Research and Development (FAPEMIG-Brazil) (Process: APQ-00554-21, APQ-00458-24). The authors are also thankful to the Rede Mineira de Materiais Inorgânicos (RM^2I), a research group supported by FAPEMIG (RED-00116-23). The authors are also thankful to FAPESP 2022/10340-2 and 2022/07231-7.

Data availability Not applicable.

Declarations

Conflict of interest The authors declare no conflicts of interest.

References

1. M.S. Safavi, F.C. Walsh, L. Visai, J. Khalil-Allafi, ACS Omega. **7**, 9088–9107 (2022). https://doi.org/10.1021/acsomega.2c00440
2. M.U. Khalid, A. Rudokaite, A.M.H. da Silva, M. Kirsnyte-Snioke, A. Stirke, W.C. Melo, Nanomaterials. **15**, 106 (2025). https://doi.org/10.3390/nano15020106
3. Plano Estadual da Mineração, Diagnóstico do Setor Mineral de Minas Gerais. Available online: https://ibram.org.br/wp-content/uploads/2021/02/PEM-MG.pdf. Accessed 28 November 2024
4. J.P.L. Nascimento, G.T.L. Teixeira, M.M.S. Obata, M.V. Silva, C.J.F. Oliveira, L.E.A. Silva, R.V. Gelamo, N.B.L. Slade, J.A. Moreto, Mater. Res. **26**, e20230251 (2023). https://doi.org/10.1590/1980-5373-MR-2023-0251
5. J.A. Moreto, R.V. Gelamo, M.V. da Silva, T.T. Steffen, C.J.F. de Oliveira, P.A. de Buranello, M.R. Pinto, J. Mater. Sci: Mater. Med. **32** (2021). https://doi.org/10.1007/s10856-021-06498-7
6. M.C. de Almeida Bino, W.A. Eurídice, R.V. Gelamo, N.B. Leite, M.V. da Silva, A. de Siervo, M.R. Pinto, P.A. de Buranello, J.A. Moreto, Appl. Surf. Sci. **557**, 149739 (2021). https://doi.org/10.1016/j.apsusc.2021.149739
7. N.H. Marins, R.M. Silva, C.P. Ferrua, D. Łukowiec, A.M. Barbosa, J.S. Ribeiro, F. Nedel, E.R. Zavareze, T. Tański, N.L.V.

Carreño, J. Biomed. Mater. Res. B Appl. Biomater. **108**, 1559–1567 (2020). https://doi.org/10.1002/jbm.b.34503
8. N.H. Marins, C.T. Meereis, R.M. Silva, C.P. Ruas, A.S. Takimi, N.L. Carreño, F.A. Ogliari, Polym. Bull. **75**, 2301–2314 (2018). https://doi.org/10.1007/s00289-017-2150-8
9. T.A.V. Pereira, Nanopartículas de óxidos de ferro e nióbio com diferentes recobrimentos: síntese, caracterização e avaliação do potencial biológico. PhD Thesis. University of São Paulo, São Paulo (2018). https://doi.org/10.11606/T.46.2019.tde-16042019-084916
10. J.V. Formica, W. Regelson, Food Chem. Toxicol. **33**, 1061–1080 (1995). https://doi.org/10.1016/0278-6915(95)00077-1
11. G.E.S. Batiha, A.M. Beshbishy, M. Ikram, Z.S. Mulla, M.E.A. El-Hack, A.E. Taha, A.M. Algammal, Y.H. Elewa, Foods. **9**, 374 (2020). https://doi.org/10.3390/foods9030374
12. A. Rauf, M. Imran, I.A. Khan, M. ur-Rehman, S.A. Gilani, Z. Mehmood, M.S. Mubarak, Phytother Res. **32**, 2109–2130 (2018). https://doi.org/10.1002/ptr.6155
13. K.T. Chung, T.Y. Wong, C.I. Wei, Y.W. Huang, Y. Lin, Crit. Rev. Food Sci. Nutr. **38**, 421–464 (1998). https://doi.org/10.1080/10408699891274273
14. A. Baldwin, B.W. Booth, J. Biomater, Appl. **36**, 1503–1523 (2022). https://doi.org/10.1177/08853282211058099
15. B. Kaczmarek, Materials. **13**, 3224 (2020). https://doi.org/10.3390/ma13143224
16. A. Hacısevki, J. Fac. Pharm. Ankara. **38**, 233–255 (2009). https://doi.org/10.1501/Eczfak_0000000528
17. A. Ali, S. Riaz, W. Khalid, M. Fatima, U. Mubeen, Q. Babar, M.F. Manzoorg, M.Z. Khalidi, F.K. Madilo, Int. J. Food Prop. **27**, 493–515 (2024). https://doi.org/10.1080/10942912.2024.2327335
18. W.M. Abdelraheem, M.M. Refaie, R.K.M. Yousef, A.S. Abd, El Y.M. Fatah, R. Mousa, Rashwan, Front. Microbiol. **13**, 847449 (2022)
19. D. Mechi, B. Baccouri, D. Martín-Vertedor, L. Abaza, Molecules. **28**, 707 (2023). https://doi.org/10.3390/molecules28020707
20. J. Bié, B. Sepodes, P.C. Fernandes, M.H. Ribeiro, Compounds. **3**, 40–72 (2023). https://doi.org/10.3390/compounds3010005
21. W. Baer-Dubowska, H. Szaefer, A. Majchrzak-Celińska, V. Krajka-Kuźniak, Curr. Pharmacol. Rep. **6**, 28–37 (2020). https://doi.org/10.1007/s40495-020-00211-y
22. X. Cai, Z. Fang, J. Dou, A. Yu, G.J.C.M.C. Zhai, Curr. Med. Chem. **20**, 2572–2582 (2013). https://doi.org/10.2174/09298673113209990120
23. S. Abbas, C. Da Wei, K. Hayat, Z. Xiaoming, Food Rev. Int. **28**, 343–374 (2012). https://doi.org/10.1080/87559129.2011.635390
24. B. Omran, K.H. Baek, Molecules. **26**, 7031 (2021). https://doi.org/10.3390/molecules26227031
25. L.E. Shi, X.F. Guo, X.J. Fang, L.M. Zhao, Y.X. Liang, M. Chen, Z.X. Tang, D.S. Zhu, J. Chem. Soc. Pak. 33, 929–934 (2011). http://142.54.178.187:9060/xmlui/handle/123456789/19801
26. L.F. Dalmolin, N.M. Khalil, R.M. Mainardes, Mater. Sci. Eng. C **62**, 1–8 (2016). https://doi.org/10.1016/j.msec.2016.01.031
27. D.M. Faria, S.M. Dourado, J.P.L. Júnior, E.D.S. Nascimento, R.P. Nunes, L.S. Marques, J.A. Rossino, Moreto, Mat. Res. **20**, 225–235 (2016). https://doi.org/10.1590/1980-5373-MR-2016-0443
28. S.M. Dourado Junior, E.S. Nunes, R.P. Marques, L.S. Rossino, F.J. Quites, J.R. Siqueira Junior, J.A. Moreto, Mater. Sci. **52**, 9491–9507 (2017). https://doi.org/10.1007/s10853-017-1103-9
29. G.G. Slade, S.M. Dourado Junior, R.J. Oliveira, J.A. Moreto, Mat. Res. **22**, e20190306 (2019). https://doi.org/10.1590/1980-5373-MR-2019-0306
30. C.G. Oliveira, L.F. Dalmolin, R.T.C. Silva, R.F. Lopez, P.I.S. Maia, J.A. Moreto, New. J. Chem. **44**, 14928–14935 (2020)
31. L.A. Mendes, R.P. Marques, S.A. Silva, N.B.L. Slade, K. Schwarz, J.A. Moreto, Orbital: Electron. J. Chem. **12**, 291–296 (2020). https://doi.org/10.17807/orbital.v12i4.1552
32. L. Custódio, L.A. Mendes, D.S. Alvares, J.A. Moreto, N.B.L. Slade, Bull. Mater. Sci. **45**, 159 (2022). https://doi.org/10.1007/s12034-022-02734-0
33. L.A. Mendes, T.S. Farnesi-de-Assunção, P.A. Oliveira, I.S. Rotta, J.A. Moreto, K.R. Devienne, A.D. Paiva, N.B.L. Slade, Nano Trends. **7**, 100040 (2024). https://doi.org/10.1016/j.nwnano.2024.100040
34. W. Fan, Q. Zhang, W. Deng, Y. Wang, Chem. Mater. **25**, 3277–3287 (2013). https://doi.org/10.1021/cm400192q
35. M. Hara, Bull. Chem. Soc. Jpn. **87**, 931–941 (2014). https://doi.org/10.1246/bcsj.20140131
36. M.L. Marin, G.L. Hallett-Tapley, S. Impellizzeri, C. Fasciani, S. Simoncelli, J.C. Netto-Ferreira, J.C. Scaiano, Catal. Sci. Technol. **4**, 3044–3052 (2014). https://doi.org/10.1039/C4CY00238E
37. K. Skrodczky, M.M. Antunes, X. Han, S. Santangelo, G. Scholz, A.A. Valente, N. Pinna, P.A. Russo, Commun. Chem. **2**, 129 (2019). https://doi.org/10.1038/s42004-019-0231-3
38. Y. Fu, C.J. Neal, E. Kolanthai, J. Wojewoda-Budka, N. Sobczak, L. Lityńska-Dobrzyńska, I. Patel, S. Seal, Surf. A: Physicochem Eng. Asp. **699**, 134603 (2024). https://doi.org/10.1016/j.colsurfa.2024.134603
39. S. Patra, C. Davoisne, S. Bruyère, H. Bouyanfif, S. Cassaignon, P.L. Taberna, F. Sauvage, Part. Syst. Charact. **30**, 1093–1104 (2013). https://doi.org/10.1002/ppsc.201300178
40. J. Lv, S. Wu, Z. Tian, Y. Ye, J. Liu, C. Liang, J. Mater. Chem. A **7**, 12627–12634 (2019). https://doi.org/10.1039/C9TA02045D
41. G. Rodríguez-Gattorno, P. Santiago-Jacinto, L. Rendon-Vázquez, J. Németh, I. Dékány, D. Díaz, J. Phys. Chem. B **107**, 12597–12604 (2003). https://doi.org/10.1021/jp035788x
42. S.T. Shah, W.A. Yehye, O. Saad, K. Simarani, Z.Z. Chowdhury, A.A. Alhadi, L.A. Al-Ani, Nanomaterials. **7**, 306 (2017). https://doi.org/10.3390/nano7100306
43. S.T. Shah, W.A. Yehye, Z.Z. Chowdhury, K. Simarani, PeerJ 7, e7651 (2019). https://doi.org/10.7717/peerj.7651
44. G.T.L. Teixeira, R.V. Gelamo, M.M.S. Obata, L.E. Andrade Silva, M.V. Silva, C.J.F. Oliveira, N.B.L. Slade, Biofouling. **39**, 47–63 (2023). https://doi.org/10.1080/08927014.2023.2183121
45. N.B. Leite, D. dos Santos Alvares, B.M. de Souza, M.S. Palma, J. Ruggiero Neto, Eur. Biophys. J. **43**, 121–130 (2014). https://doi.org/10.1007/s00249-014-0945-1
46. ISO 10993-5, 2009. Biological evaluation of medical devices-part 5: tests for in vitro cytotoxicity. International Organization for Standardization (2009)
47. CLSI, *Performance Standards for Antimicrobial Susceptibility Testing*, 33rd edn. (CLSI supplement M, Wayne PA, 2023), p. 100
48. CLSI, *Performance Standards for Antimicrobial Susceptibility Testing*, 30th edn. (CLSI supplement M, Wayne PA, 2020), p. 100
49. K.R. Rocha, H.F. Perini, C.M. de Souza, J. Schueler, N.F. Tosoni, M.C. Furlaneto, L. Furlaneto-Maia, World J. Microbiol. Biotechnol. **35**, 96 (2019). https://doi.org/10.1007/s11274-019-2675-0
50. N. Odzak, D. Kistler, R. Behra, L. Sigg, Environ. Pollut. **191**, 132–138 (2014). https://doi.org/10.1016/j.envpol.2014.04.010
51. A.M. Studer, L.K. Limbach, L. Van Duc, F. Krumeich, E.K. Athanassiou, L.C. Gerber, H. Moch, W.J. Stark, Toxicol. Lett. **197**, 169–174 (2010). https://doi.org/10.1016/j.toxlet.2010.05.012
52. X. Chen, T. Yu, X. Fan, H. Zhang, Z. Li, J. Ye, Z. Zou, Appl. Surf. Sci. **253**, 8500–8506 (2007). https://doi.org/10.1016/j.apsusc.2007.04.035
53. T. Fuchigami, K.I. Kakimoto, J. Mater. Res. **32**, 3326–3332 (2017). https://doi.org/10.1557/jmr.2017.200
54. G. Dehghan, Z. Khoshkam, Food Chem. **131**, 422–426 (2012). https://doi.org/10.1016/j.foodchem.2011.08.074

55. S. Ambreen, N.D. Pandey, A. Chouhan, H. Kumar, A. Pandey, J. Sol-Gel Sci. Technol. **98**, 319–334 (2021). https://doi.org/10.1007/s10971-021-05514-0
56. N. Uekawa, T. Kudo, F. Mori, Y.J. Wu, K. Kakegawa, J. Colloid Interface Sci. **264**, 378–384 (2003). https://doi.org/10.1016/S0021-9797(03)00460-0
57. M. Ristić, S. Popović, S. Musić, Mater. Lett. **58**, 2658–2663 (2004). https://doi.org/10.1016/j.matlet.2004.03.041
58. B.H. Stuart, *Infrared Spectroscopy: Fundamentals and Applications; ANTS (Analytical Techniques in the Sciences) Series*, 1st edn. (Wiley, New York, 2004)
59. P.A. Burke, E.I. Ko, J. Catal. **129**, 38–46 (1991). https://doi.org/10.1016/0021-9517(91)90007-Q
60. L.A. Rodrigues, Síntese de nanopartículas de óxido de nióbio hidratado via microemulsão inversa. Master's Thesis. University of São Paulo, Lorena (2009). https://doi.org/10.11606/D.97.2009.tde-03102012-121612
61. J.R. Ferraro, *Low-frequency Vibrations of Inorganic and Coordination Compounds*, 1st edn. (Springer, New York, 2012)
62. R.G. Engel, G.S. Kriz, G.M. Lampman, D.L. Pavia, *Introduction To Organic Laboratory Techniques: Small Scale Approach*, 3rd edn. (Cengage Learning, Boston, 2011)
63. G.M. Bousada, V.N. da Silva, B.F. de Souza, R.S. de Oliveira, I.M. Junior, C.H.F. da Cunha, D. Astruc, R.R. Teixeira, R.P.L. Moreira, RSC Adv. **14**, 19459–19471 (2024). https://doi.org/10.1039/D4RA01879F
64. D.L. Pavia, G.M. Lampman, G.S. Kriz, J.R. Vyvyan, *Introduction To Spectroscopy*, 4th edn. (Cengage Learning, Boston, 2008)
65. L.F.W. Brum, M.D.C.R. da Silva, C. dos Santos, G. Pavoski, D.C.R. Espinosa, W.L. da Silva, Catal. Today. **445**, 115106 (2025). https://doi.org/10.1016/j.cattod.2024.115106
66. A.M. Raba, J. Bautista-Ruíz, M.R. Joya, Mat. Res. **19**, 1381–1387 (2016). https://doi.org/10.1590/1980-5373-MR-2015-0733
67. J.M. Jehng, I.E. Wachs, Chem. Mater. **3**, 100–107 (1991). https://doi.org/10.1021/cm00013a025
68. V. Lebarbier, M. Houalla, T. Onfroy, Catal. Today. **192**, 123–129 (2012). https://doi.org/10.1016/j.cattod.2012.02.061
69. C. Zhong, S. Tan, T. Langrish, J. Food Eng. **244**, 11–20 (2019). https://doi.org/10.1016/j.jfoodeng.2018.09.020
70. R.W. Berg, Appl. Spectrosc. Rev. **50**, 193–239 (2014). https://doi.org/10.1080/05704928.2014.952431
71. A. Espina, M.V. Cañamares, Z. Jurasekova, S. Sanchez-Cortes, ACS Omega. **7**, 32, 27937–27949 (2022). https://doi.org/10.1021/acsomega.2c01679
72. Y. Numata, H. Tanaka, Food Chem. **126**, 751–755 (2011). https://doi.org/10.1016/j.foodchem.2010.11.059
73. M. Vosoughifar, J. Mater. Sci: Mater. Electron. **28**, 532–536 (2017). https://doi.org/10.1007/s10854-016-5555-5
74. N. Kumari, S.K. Samdarshi, R. Verma, K. Gaurav, A.S. Bhattacharyya, K. Mohanty, U. Deshpande, Environ. Sci. Pollut Res. **30**, 122458–122469 (2023). https://doi.org/10.1007/s11356-023-31001-w
75. N. Kumari, K. Gaurav, S.K. Samdarshi, A.S. Bhattacharyya, S. Paul, B. Rajbongshi, K. Mohanty, Sol Energy Mater. Sol Cells. **208**, 110408 (2020). https://doi.org/10.1016/j.solmat.2020.110408
76. A.C.H. Barreto, V.R. Santiago, S.E. Mazzetto, J.C. Denardin, R. Lavín, G. Mele, M.E.N.P. Ribeiro, I.G.P. Vieira, T. Gonçalves, N.M.P.S. Ricardo, P.B.A. Fechine, J. Nanopart. Res. **13**, 6545–6553 (2011). https://doi.org/10.1007/s11051-011-0559-9
77. N.A. Dsouki, M.P. de Lima, R. Corazzini, T.M. Gáscon, L.A. Azzalis, V.B.C. Junqueira, D. Feder, F.L.A. Fonseca, J. Mater. Sci. Mater. Med. **25**, 1301–1305 (2014). https://doi.org/10.1007/s10856-014-5153-0
78. V. Lobo, A. Patil, A. Phatak, N. Chandra, Pharmacogn Rev. **4**, 118 (2010). https://doi.org/10.4103/0973-7847.70902
79. B. Halliwell, Biochem. Soc. Symp. **61**, 73–101 (1995). https://doi.org/10.1042/bss0610073
80. I.S. Young, J.V. Woodside, J. Clin, Pathol. **54**, 176–186 (2001). https://doi.org/10.1136/jcp.54.3.176
81. S. Miquel, R. Lagrafeuille, B. Souweine, C. Forestier, Front. Microbiol. **7**, 592 (2016). https://doi.org/10.3389/fmicb.2016.00592
82. J.P. McEvoy, K. Genc, P. Loi, W.J. Walker, in Nanoparticles in Biology and Medicine, ed. by E. Ferrari, M. SolovievHumana, New York, (2020). https://doi.org/10.1007/978-1-0716-0319-2_2
83. D. Li, S. Chen, K. Zhang, N. Gao, M. Zhang, G. Albasher, J. Shi, C. Wang, Sci. Rep. **11**, 1703 (2021). https://doi.org/10.1038/s41598-021-81305-5